The Iranian Journal of Mechanical Engineering Transactions of ISME
Journal homepage: https://jmee.isme.ir/
Vol. 25, No. 2, 2024, pp. 93-113

Research Paper

DOI: https://doi.org/10.30506/jmee.2024.2023842.1342

Elasto-plastic Analysis of Thick Cylinders using Shear Deformation Theories and Radial Return Mapping Method

Mojtaba Ghadimi[*]
Ph.D. Candidate

Mehdi Ghannad[†]
Professor

In this paper, the elasto-plastic stress analysis of the axisymmetric thick cylindrical shells undergoing internal pressure is investigated. The displacement field is considered according to first-order and higher-order shear deformation theories. The material is supposed to be elastic-perfectly plastic and the von Mises yield criterion is considered to determine the state of stress. The radial return method is applied to obtain the plastic stress components in the plastic region. Finally, the problem is solved for a thick cylindrical shell under internal pressure which is fixed at both ends and the results are compared with finite element results. The stresses, displacement, and elastic limit pressure results are indicated the effectiveness of higher-order shear deformation theory than first-order shear deformation theory.

Keywords: Elastic-perfectly plastic, Plane elasticity theory, Radial return method, Shear deformation theories

1 Introduction

Cylindrical shells are the principal structural elements of various structures. These structures are used frequently in many engineering applications, such as pressure vessels for transporting or storing highly pressurized liquids or gases, nuclear reactors, military applications, aerospace industries, etc. Researchers have studied the behaviour of the thick-walled cylinders subjected to loads. They have not only focused on the elastic behavior of the cylindrical structure but have extended their studies to the elasto-plastic behavior to decrease the usage of the material and to reduce the cost of a structure by optimizing the design of the cylinders.

[*]Ph.D. Candidate, Department of Mechanical Engineering, Shahrood University of Technology, Shahrood, Iran, moghadimi@yahoo.com

[†]Corresponding author, Professor, Department of Mechanical Engineering, Shahrood University of Technology, Shahrood, Iran, mghannadk@shahroodut.ac.ir & Ghannad.mehdi@gmail.com

Received: 2024/02/26, Revised: 2024/05/22, Accepted: 2024/07/01

There are several approaches to dealing with the elastic part of thick cylindrical shells and finding the equilibrium equations of the problem. The simplest way is to use the classic theory known as plane elasticity theory (PET) [1-3]. PET can only be appropriate for stress and displacement analysis of the shell through the thickness and therefore is not applicable near the boundaries of the shell. Another approach that researchers apply to find the equilibrium equations of thick-walled cylindrical shells is the shear deformation theory (SDT). First time in 1958, Mirsky and Hermann [4] employed the first-order shear deformation theory (FSDT) to analysis of isotropic cylinders. Later on, Reddy and Liu in 1985 [5] developed a third-order shear deformation theory. They supposed that the transverse shear strains to be distributed parabolically through the shell. Ghannad and Zamani-Nejad [6] used FSDT to study the behavior of the thick heterogeneous cylinders subjected to uniform loading. They used virtual work principle to derive the governing equations of an axisymmetric cylinder. Eipakchi et al. [7] investigated the governing equations of homogeneous cylinders with variable thickness using FSDT and represent the solution of the equations using perturbation theory. Furthermore, they applied matched asymptotic expansion method for stress analysis of an axisymmetric thick conical shell subjected to non-uniform pressures according to shear deformation theories [8]. Gharooni and Ghannad [9] analyzed thick variable thickness cylinders made of functionally graded material and clamped boundary conditions subjected to non-uniform loading. They derived the governing equilibrium equations based on FSDT. They also solved the problem of radially functionally graded materials [10].

There are some works on the elasto-plastic analysis of disks, shafts, and shells under simplified hypotheses based on different theories. Nadai [11] analyzed the perfectly plastic rotating cylinders under the assumption of incompressibility. Chakrabarty [12] presented the analytical solution for the elasto-plastic expansion of a cylindrical tube subjected to internal pressure according to Tresca and von Mises yield criteria. He assumed the tube is so large that plane transverse sections remain plane during the expansion. Eraslan [13] studied the elasto-plastic deformations of a rotating shaft based on the Tresca yield condition. He solved the problem for both fixed and both free ends condition of the shaft. Eraslan [14] investigated the analytical solutions to find the stress distribution of rotating parabolic solid disks based on the Tresca yield criterion and its associated flow rule. He considered the disk is plane stress and made of linear strain hardening material. An elasto-plastic analysis of the rotating cylinder subjected to mechanical loading and unloading under plane strain conditions was investigated by Prokudin [15]. The elasto-plastic analysis of a functionally graded rotating disk was studied by Zamani-Nejad and Rastgoo [16] using the elastic-perfectly plastic material model. They employed the Tresca yield criterion. The analysis is based on the Tresca yield condition and perfectly plastic material behavior. Elasto-plastic solutions for double-layered and multilayered combined thick-walled cylinders under internal pressure were studied by Zhu et al. [17]. They used the unified strength theory that considers the influence of the intermediate principal stress and strength difference. Temesgen et al. [18] performed an analytical solution for elasto-plastic analysis of a functionally graded rotating cylinder under uniform pressure and radial temperature gradient using the Seth transition theory which is not needed yield criterion, material incompressibility, or infinitesimally small deformation assumptions.

The class of elastic-predictor plastic-corrector algorithms is based on a two-step scheme: (i) an elastic trial state is first computed; (ii) then, if the onset of plasticity is detected, a plastic correction is computed using the trial state as the initial condition to update all the internal variables [19]. The idea of such a scheme traces back to Wilkins [20] who proposed the radial-return method for the von Mises perfect plasticity. The superiority of the radial return mapping method compared to other return schemes is established in [21, 22]. Dunne and Petrinic [23] used an implicit integration scheme called the radial return method which is obtained based on von Mises plasticity. They used the normality hypothesis of plasticity and

the associated flow rule for the von Mises criterion to formulate the problem in the plastic region. Widlak [24] presented the radial return method for elasto-plastic constitutive equations in the special case of analysis of a thick-walled cylinder. The robustness and step-size insensitivity of this integration method was proved and efficient solution strategies were chosen.

The present study deal with the elasto-plastic stress analysis of the thick-walled cylindrical shell structure. To solve the problem some assumptions have been made such as the displacement field considered based on shear deformation theory and the cylinder supposed made of elastic-perfectly plastic material. The von Mises yield criterion and Prandtl-Reuss flow rule are applied to find the cylinder behavior in the plastic region. The case study solved for a clamped-clamped thick cylinder subject to uniform internal pressure and the elastic limit internal pressure of the cylinder was found based on PET, FSDT, and HSDT. The differences and effectiveness of each theory are investigated for a clamped-clamped cylindrical shells. Moreover, the elasto-plastic stresses of the cylinder are illustrated at the different surfaces and the results are compared with the Abaqus finite element method (FEM) results.

2 Description of the problem

Figure (1a) shows a schematic of a cylindrical shell with the inner radius of r_i, the outer radius of r_o, the thickness of h, and length of L. The position of any typical point m of the cylindrical shell can be defined as follows:

$$\begin{gathered} m: (r\,, x) = (R + z\,, x) \\ -h/2 \le z \le +h/2 \quad , \quad 0 \le x \le L \end{gathered} \tag{1}$$

Where R and z denote the radius of the mid-plane and the distance from the mid-plane, respectively. As shown in Figure (1b) the cylinder is supposed to be clamped at both ends and subjected to the internal pressure P.

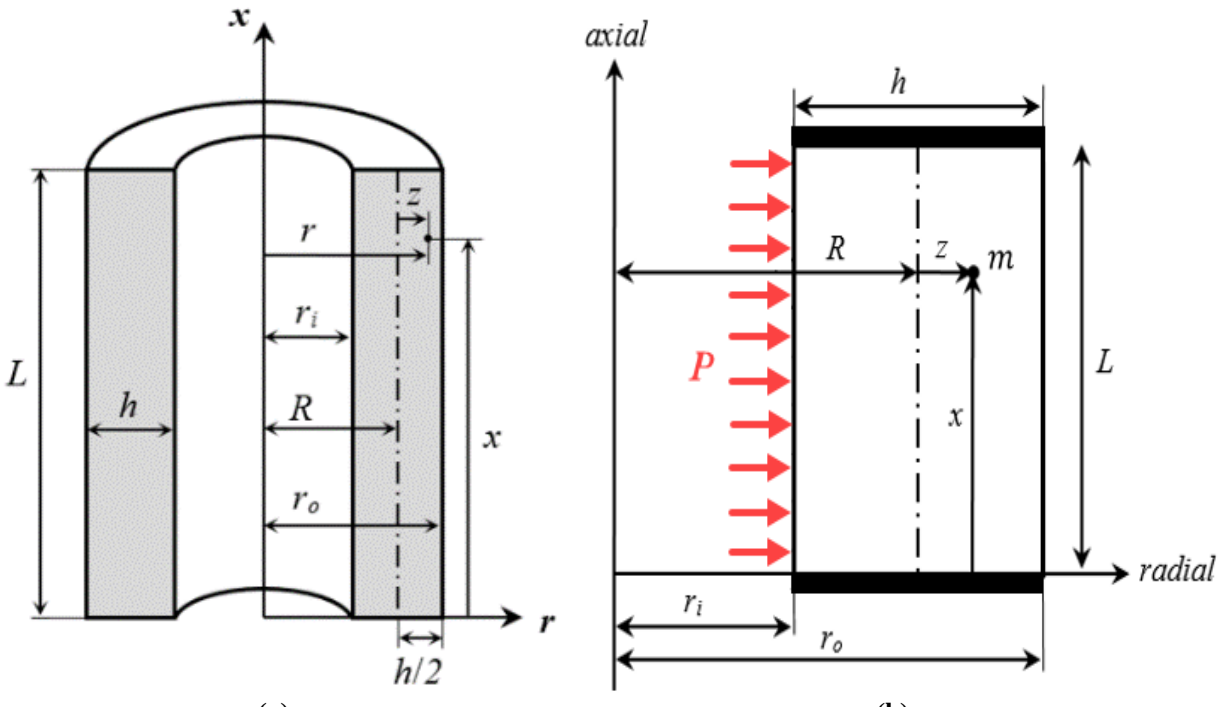

(**a**) (**b**)

Figure 1 The schematic of the cylindrical shell, (**a**) Geometry parameters, (**b**) Boundary and loading conditions.

3 Elasto-plastic solution of the cylinder

In this section the elasto-plastic stress analysis of the cylinder is present using PET, FSDT, and HSDT. It is assumed that the material is non-strain hardening and consequently yield strength is equal to a constant value. The maximum distortion criterion known as von Mises yield criterion is used to define the state of stress.

3.1 Plane elasticity theory (PET)

Using PET for both closed-end cylinders subjected to internal pressure, the radial, circumferential (hoop), and axial (longitudinal) stresses are obtained by Lame's theorem [3] as follows, respectively:

$$\sigma_r = \frac{P}{k^2-1}\left(1-\frac{k^2}{\bar{r}^2}\right), \qquad \sigma_\theta = \frac{P}{k^2-1}\left(1+\frac{k^2}{\bar{r}^2}\right), \qquad \sigma_x = \frac{2\nu P}{k^2-1} \tag{2}$$

Here $k = r_0/r_i,\ \bar{r} = r/r_i$, and ν is the Poisson's ratio of the cylinder material.
From Eq. (2) it is obvious that the highest amounts of σ_r and σ_θ are achieved on the inner surface of the pressurized cylinder. It can be expected therefore that if these stresses reach critical values, the yielding will occur at the inner surface.
The most commonly used in engineering practice, particularly for computational analysis, is the von Mises criteria, which relies on the knowledge of effective stress. In terms of direct and shear stresses, the effective stress for the full axisymmetric cylindrical shell based on von Mises failure theory is defined as [25]:

$$\sigma_e \equiv \frac{1}{\sqrt{2}}\left[(\sigma_z-\sigma_\theta)^2 + (\sigma_\theta-\sigma_x)^2 + (\sigma_z-\sigma_x)^2 + 6\tau_{zx}^2\right]^{1/2} \tag{3}$$

In addition, the yield function for the material without hardening is defined by [25]:

$$f = \sigma_e - \sigma_y \tag{4}$$

Here σ_y is the yield stress. In the above equation, if $f<0$ the material experience elastic deformation, while if $f=0$ the material experience plastic deformation.
For PET the shear stresses are assumed to be zero. Thus, σ_r, σ_θ, and σ_x are being the principal stresses. The plastic deformation starts when the yield function becomes zero. Hence:

$$(\sigma_r-\sigma_\theta)^2 + (\sigma_\theta-\sigma_x)^2 + (\sigma_x-\sigma_r)^2 = 2{\sigma_y}^2 \tag{5}$$

Substituting Eq. (2) into Eq. (5), the elastic limit pressure (P_c) of the shell subjected to internal pressure based on the von Mises criterion for both closed-end cylinders, is obtained as:

$$P_c = \sigma_y(k^2-1)\{(1-2\nu)^2 + 3k^4\}^{-1/2} \tag{6}$$

3.2 Shear deformation theory (SDT)

The displacement field for an axisymmetric cylindrical shell (U_x, U_θ, U_z) is assumed to be a function of z and x; which are expressed based on FSDT and HSDT as follows [26]:

$$\begin{cases} U_x(x,z) = \sum u_x^i(x) z^i \\ U_\theta(x,z) = 0 \\ U_z(x,z) = \sum u_z^i(x) z^i \end{cases}, \quad FSDT(i=0,1)\ ,\ HSDT\ (i=0,1,2,3) \tag{7}$$

Where $u_x^0\ (x)$ and $u_z^0\ (x)$ are the displacement components of the middle surface. Also, $u_x^i\ (x)$ and $u_z^i\ (x)$ are the components used to determine the displacement change field.
In addition, the strain-displacement relations (constitutive equations) [26] are used to obtain the strain tensor components:

$$\varepsilon_x = \frac{\partial U_x(x,z)}{\partial x}, \quad \varepsilon_\theta = \frac{U_z(x,z)}{r}, \quad \varepsilon_z = \frac{\partial U_z(x,z)}{\partial z}, \quad \gamma_{xz} = \frac{\partial U_x(x,z)}{\partial z} + \frac{\partial U_z(x,z)}{\partial x} \tag{8}$$

Using the stress-strain relations, the stress tensor for the isotropic cylindrical shell is written as [26]:

$$\begin{bmatrix} \sigma_x \\ \sigma_\theta \\ \sigma_z \\ \tau_{xz} \end{bmatrix} = \lambda \begin{bmatrix} 1-\nu & \nu & \nu & 0 \\ \nu & 1-\nu & \nu & 0 \\ \nu & \nu & 1-\nu & 0 \\ 0 & 0 & 0 & \frac{1-2\nu}{2} \end{bmatrix} \begin{Bmatrix} \varepsilon_x \\ \varepsilon_\theta \\ \varepsilon_z \\ \gamma_{xz} \end{Bmatrix}, \quad \lambda = \frac{E}{(1+\nu)(1-2\nu)} \tag{9}$$

Where E denotes Young's Modulus. The stress resultants are as follows [26]:

$$\begin{Bmatrix} N_x^i \\ N_\theta^i \\ N_z^i \\ N_{xz}^i \end{Bmatrix} = \int_{-\frac{h}{2}}^{\frac{h}{2}} \begin{Bmatrix} \sigma_x(1+z/R) \\ \sigma_\theta R \\ \sigma_z(1+z/R) \\ K\tau_{xz}(1+z/R) \end{Bmatrix} z^i\, dz, (i=0,1,2,3) \tag{10}$$

Only the first two terms of the stress resultants are used for FSDT. In Eq. (10), for shear stress terms (N_{xz}^i), K is the shear correction factor used for FSDT. It is assumed for cylindrical shells $K = 5/6$ [11] [11]. It is clear that based on the nature of the HSDT that can cover the shear deformation parabolically through the thickness, the shear correction factor is not needed. Hence, K takes the value equal to one in stress resultants associated with HSDT.
Strain energy and external work can be written as:

$$U = \iiint_V \frac{1}{2}(\sigma_x\varepsilon_x + \sigma_\theta\varepsilon_\theta + \sigma_z\varepsilon_z + \tau_{xz}\gamma_{xz})dV, \quad W = \iint_S (\vec{f}_{sf}.\vec{u})dS \tag{11}$$

The variations of strain energy (δU) and the variations of external work (δW) for the shell subjected to the internal pressure are expanded as [26]:

$$\delta U = 2\pi \int_0^L \int_{-h/2}^{h/2} (\sigma_x \delta\varepsilon_x + \sigma_\theta \delta\varepsilon_\theta + \sigma_z \delta\varepsilon_z + \tau_{xz}\delta\gamma_{xz})(R+z)dzdx$$
$$\delta W = 2\pi \left[\int_0^L (P\delta U_z)\left(R - \frac{h}{2}\right)dx \right] \tag{12}$$

Rewrite the stress and strain tensor components in the form of displacement into Eq. (12), and based on the calculus of variation and virtual work principle (δU = δW), with consider the Eq. (10), the governing equations for HSDT are obtained as [26]:

$$\frac{d}{dx}\left(RN_x^i\right) - iRN_{xz}^{i-1} = 0$$
$$\frac{d}{dx}\left(RN_{xz}^i\right) - iRN_z^{i-1} - N_\theta^i = -P\left(R - \frac{h}{2}\right)\left(-\frac{h}{2}\right)^i \qquad (i = 0,1,2,3) \tag{13}$$

It is noteworthy that the set of equations for FSDT is obtained, by putting i = 0,1 in Eq. (13). The boundary conditions for HSDT are as follows [26]:

$$R\left[\sum_{i=0}^{3} N_x^i \delta U_x^i + \sum_{i=0}^{3} N_{xz}^i \delta U_z^i\right]_{0,L} = 0 \qquad (i = 0,1,2,3) \tag{14}$$

Substituting Eq. (10) into Eq. (13) and doing some calculations, the governing equations for HSDT are obtained in the displacements form as follows:

$$[\bar{A}]\frac{d^2}{dx^2}\{\bar{y}\} + [\bar{B}]\frac{d}{dx}\{\bar{y}\} + [\bar{C}]\{\bar{y}\} = \{\bar{F}\}$$
$$\{\bar{y}\} = \{u_x^0 \quad u_x^1 \quad u_x^2 \quad u_x^3 \quad u_z^0 \quad u_z^1 \quad u_z^2 \quad u_z^3\}^T \tag{15}$$

\

In Eq. (15), [$\bar{A}$], [$\bar{B}$], and [$\bar{C}$] are the coefficients matrices of order eight for HSDT. The coefficient matrices are in order four, for FSDT. In addition, { $\bar{F}$ } is the force matrix. Eq. (15) is the set of differential equations and to solve these equations, the reverse of [$\bar{C}$] is needed, which is irreversible. To overcome this problem, by putting du_x^0/dx instead of u_x^0 and integrating from the first equation represents in Eq. (13), it is obtained:

$$RN_x = C_0 \tag{16}$$

Therefore, the set of Eq. (15) is changed as follows:

$$[A]\frac{d^2}{dx^2}\{y\} + [B]\frac{d}{dx}\{y\} + [C]\{y\} = \{F\}$$
$$\{y\} = \{du_x^0/dx \quad u_x^1 \quad u_z^0 \quad u_z^1\}^T \quad \text{for FSDT}$$
$$\{y\} = \{du_x^0/dx \quad u_x^1 \quad u_x^2 \quad u_x^3 \quad u_z^0 \quad u_z^1 \quad u_z^2 \quad u_z^3\}^T \quad \text{for HSDT} \tag{17}$$

The coefficient matrices and the force matrix for FSDT and HSDT can be determined as Appendix A and B, respectively.

The differential Eq. (17) has the solution including general solution $\{y\}_g$ and particular solution $\{y\}_p$ as:

$$\{y\} = \{y\}_g + \{y\}_p \tag{18}$$

For the general solution for homogeneous case, $\{y\}_g = \{V\}e^{mx}$ is substituted in Eq. (17) and it is obtained:

$$e^{mx}[m^2[A] + m[B] + [C]]\{V\} = \{0\} \tag{19}$$

Eq. (19) is an eigenvalue problem for non-trivial solution $e^{mx} \neq 0$, the determinant of the coefficient must be considered to be zero.

$$\det[m^2[A] + m[B] + [C]]\{V\} = 0 \tag{20}$$

For FSDT the above determinant leads to an eight-order polynomial which is a function of m. Eight eigenvalues m_i achieve from the solution of Eq. (20) contains three pairs of conjugated roots and one pair of zero roots. Also, Eq. (20) leads to a sixteen order polynomial which contain seven pairs of conjugated roots and one pair of zero roots for HSDT.
By calculating eigenvectors $\{V\}_i$ correspond to eigenvalues, the general solution of Eq. (17) for HSDT is written as:

$$\{y\}_g = \sum_{i=1}^{14} C_i \{V\}_i e^{m_i x} \tag{21}$$

The constants C_i are obtained by applying boundary conditions.
The particular solution for Eq. (17) is obtained as follows:

$$\{y\}_p = [C]^{-1}\{F\} \tag{22}$$

Thus the solution of Eq. (17) for HSDT is achieved by summation of general and particular solutions as:

$$\begin{gathered} \{y\} = \{y\}_g + \{y\}_p \\ \{y\} = \sum_{i=1}^{14} C_i \{V\}_i e^{m_i x} + [C]^{-1}\{F\} \end{gathered} \tag{23}$$

Finally, u_x^0 is obtained as follows:

$$u_x^0 = \int_0^L \left(\frac{du_x^0}{dx}\right) dx + C_{15} \tag{24}$$

There are sixteen constants (C_0 to C_{15}) for the case of HSDT. Sixteen boundary conditions for the clamped-clamped cylinder are obtained by putting u_x^0, u_x^1, u_x^2, u_x^3, u_z^0, u_z^1, u_z^2, u_z^3 equal to zero at each end of the cylinder ($x = 0$ and $x = L$). Similarly, it can be indicated that in the case of FSDT, there are eight constants and eight boundary conditions. After finding the displacement components, the displacement fields and consequently the strain and stress components are determined. It is assumed that the cylinder is made of elastic-perfectly plastic material. Hence, until the effective stress of any point of the shell is smaller than the yield stress the shell is elastic, otherwise, the shell became plastic.

After the shell became plastic, the von Mises stress is placed outside the yield surface. The trial stress increment, $\sigma^{tr}_{t+\Delta t}$, is outside the yield surface. At time $t + \Delta t$, the plastic corrector factor is used to update the stress and return it to the yield surface [23]. In the deviatoric plane the von Mises yield surface became the circle. Based on the normality condition of the yield surface the plastic corrector factor towards the center of the circle. Hence, this procedure is known as the radial return method. After this, all amounts are represented to be at the end of the time step. Therefore, σ is the updated stress at time $t + \Delta t$ and σ_t denotes the stress at the beginning of the time step.
Hooke's law may be expressed in the multi-axial form in terms of stress and strain tensor.

$$\tilde{\sigma} = 2G\tilde{\varepsilon}^e + \lambda \, \mathrm{tr}(\tilde{\varepsilon}^e)\tilde{I} \tag{25}$$

Where λ and G are the Lamé constants. At the end of the time step the elastic strain tensor can be written as:

$$\tilde{\varepsilon}^e = \tilde{\varepsilon}^e_t + \Delta\tilde{\varepsilon}^e = \tilde{\varepsilon}^e_t + (\Delta\tilde{\varepsilon} - \Delta\tilde{\varepsilon}^p) \tag{26}$$

Based on the incompressibility condition of plasticity ($\mathrm{tr}(\Delta\,\tilde{\varepsilon}^p) = 0$) and substituting Eq. (26) into Eq. (25), the stress at the end of the time step can be written as follows:

$$\tilde{\sigma} = 2G(\tilde{\varepsilon}^e_t + \Delta\tilde{\varepsilon}) + \lambda \, tr(\tilde{\varepsilon}^e_t + \Delta\tilde{\varepsilon})\tilde{I} - 2G\Delta\tilde{\varepsilon}^p \tag{27}$$

The first two terms of Eq. (27) are denoted as trial stress tensor ($\tilde{\sigma}^{tr}$), or elastic predictor. The third term of Eq. (27) is intended as a plastic corrector.
Based on the associated flow rule of von Mises yield criteria and the assumption of the co-directionality of plastic strain increment with normal the tangent to the yield surface, the plastic strain increment may be written as [23]:

$$\Delta\tilde{\varepsilon}^p = \frac{3}{2}\Delta p \, \frac{\tilde{\sigma}'}{\sigma_e} \tag{28}$$

In which Δp denotes the increment of effective plastic strain and $\tilde{\sigma}'$ represents the deviatoric stress tensor.
By replacing Eq. (28) with Eq. (27) and expressing the stress in its deviatoric and mean form, and rearranging Eq. (21), it is obtained:

$$\left(1 + 3G\frac{\Delta p}{\sigma_e}\right)\tilde{\sigma}' = \tilde{\sigma}^{tr} - \frac{1}{3}(\tilde{\sigma} : \tilde{I})\tilde{I} \tag{29}$$

After doing some calculations, the right side of Eq. (29) is equivalent to the deviatoric tensor of the trial stress [23] [23]. Therefore, Eq. (29) is rewritten as:

$$\left(1 + 3G\frac{\Delta p}{\sigma_e}\right)\tilde{\sigma}' = \tilde{\sigma}^{\mathrm{tr}'} \tag{30}$$

By applying the contracted tensor product for each side of Eq. (30) with itself, it is finally obtained [23]:

$$\sigma_e + 3G\,\Delta p = \sigma_e^{\mathrm{tr}} \tag{31}$$

Substituting Eq. (31) into the yield function for the elastic-perfectly plastic material (Eq. (4)), the effective plastic strain increment and more on the stress tensor can be obtained as:

$$p = \frac{\sigma_e^{\mathrm{tr}} - \sigma_y}{3G}$$
$$\tilde{\sigma} = \tilde{\sigma}^{tr} - 3G\,\Delta p\,\frac{\tilde{\sigma}'}{\sigma_e} \tag{32}$$

4 Results and discussion

In this section the elasto-plastic solution of a cylindrical shell with $r_i = 40\,mm$, $r_o = 60\,mm$, $h = 20\,mm$ and $L = 800\,mm$ is investigated. The shell is assumed to be clamped at both ends. The Poisson's ratio and Young's Modulus, have values of $\upsilon = 0.3$ and $E = 200\,GPa$, respectively. To show the effectiveness and accuracy of each method, a comparison between responses of the present theories and FEM is done. The finite element of the cylinder is performed by Abaqus. An eight-node quadratic axisymmetric element CAX8R is used to model the cylindrical shell. The boundary conditions for a clamped edge is defined by setting both the edge deflection and edge slopes equal to zero. The internal pressure applied on the inner surface of the cylinder with the desired magnitude. The twenty elements are used in the radial direction to mesh the cylinder. Convergence of finite element results in mesh refinement study accomplished by monitoring the results for different numbers of the elements in the radial direction.

Table (1) presents the elastic limit pressure (pressure that yielding begins) for FEM, PET, FSDT, and HSDT at four different lengths of the cylinder based on von Mises yield criteria. As described earlier the yielding occurs at the inner surface of the pressurized cylindrical shell. It means that the elastic limit pressure happens at the inner surface of the shell. Although away from the middle length of the cylinder the elastic limit pressure results obtained using the PET have a great agreement with the FEM results, this theory is not proper to predict the elastic limit pressure for all length of the clamped-clamped cylinder. As shown in Table (1), it is clear that the elastic limit pressure error percentage that is obtained using PET increases away from the middle length of the cylinder. In addition, it is concluded from this table that the elastic limit pressure achieved by HSDT has a reasonable agreement with the FEM results through the length of the cylinder.

The error percentage of each theory is calculated using Eq. (33) in comparison with the FEM results. In Eq. (33) $\mathrm{Q_{FEM}}$ is the parameter that achieved from FEM software and $\mathrm{Q_d}$ is the parameter of the intended theory.

$$Error\ (\%) = \left(\frac{|Q_{FEM} - Q_d|}{Q_{FEM}}\right) \times 100 \tag{33}$$

Table (2) presents the radial displacement and circumferential stress for two different lengths of the cylinder at the inner, middle, and outer surfaces of the cylinder subjected to the internal pressure of 70 MPa. The radial displacement calculated using HSDT is more accurate than PET and FSDT. In addition, the circumferential stress calculated by HSDT and PET has an appropriate agreement with the FEM results at the middle length ($\mathrm{x = L/2}$) of the cylinder. From Table (2) it is observed that the PET error percentage increases significantly away from the middle length of the cylinder ($\mathrm{x = L/10}$). Circumferential stress distribution of the clamped-clamped cylinder subjected to the internal pressure with the magnitude of 70 MPa along the length at the inner, middle, and outer surfaces of the shell are shown in Figure (2).

Table 1 Elastic limit pressure at different lengths of the cylinder

	$\mathbf{x = L/2}$		$\mathbf{x = L/4}$		$\mathbf{x = L/16}$		$\mathbf{x = L/40}$	
	Elastic limit pressure (MPa)	Error (%)	Elastic limit pressure (MPa)	Error (%)	Elastic limit pressure (MPa)	Error (%)	Elastic limit pressure (MPa)	Error (%)
FEM	79.73	---	79.74	---	87.15	---	124.50	---
PET	79.77	0.05	79.77	0.04	79.77	8.47	79.77	35.93
FSDT	97.70	22.54	97.71	22.54	97.11	11.43	153.15	23.01
HSDT	80.11	0.48	80.12	0.48	83.35	4.36	121.91	2.08

Table 2 Radial displacement and circumferential stress at two different lengths of the cylinder subjected to $P = 70\ MPa$.

		$\mathbf{x = L/2}$				$\mathbf{x = L/10}$			
		U_r (mm)	Error (%)	σ_θ (MPa)	Error (%)	U_r (mm)	Error (%)	σ_θ (MPa)	Error (%)
Inner surface	FEM	0.038700	---	181.962	---	0.039690	---	185.122	---
	PET	0.038584	0.30	182.000	0.02	0.038584	2.79	182.000	1.69
	FSDT	0.037202	3.87	206.312	13.38	0.038288	3.53	208.201	12.47
	HSDT	0.038698	0.00	183.042	0.59	0.039696	0.02	186.343	0.66
Middle surface	FEM	0.033632	---	136.624	---	0.034628	---	140.498	---
	PET	0.033488	0.43	136.640	0.01	0.033488	3.29	136.640	2.75
	FSDT	0.033476	0.47	136.166	0.34	0.034496	0.38	139.977	0.37
	HSDT	0.033622	0.03	136.000	0.02	0.034621	0.02	140.475	0.02
Outer surface	FEM	0.030749	---	111.992	---	0.031638	---	116.474	---
	PET	0.030576	0.56	112.000	0.01	0.030576	3.36	112.000	3.84
	FSDT	0.029749	3.25	89.403	20.17	0.030705	2.95	95.739	17.80
	HSDT	0.030748	0.00	111.341	0.58	0.031640	0.01	115.736	0.63

At this pressure the cylindrical shell is completely elastic for both FSDT and HSDT based on the results of the Table (1). The circumferential stress obtained with FSDT and HSDT at the middle surface of the shell (Figure (2b)) has excellent agreement with FEM results. The FSDT circumferential stress at inner and outer surfaces (Figure (2a) and Figure (2c)) of the shell has almost great differences from FEM circumferential stress. It can be concluded that by moving away from the middle surface, differences in the stresses obtained with FSDT and FEM become higher. In other words, the differences between the results predicted by FSDT decrease when the shell becomes thinner. It is observed that the results obtained based on HSDT have a compatible match with the FEM results along the length at the inner, middle, and outer surfaces of the shell. The distribution of the elastic limit pressure that yielding begins to occur based on von Mises criteria along the length of the shell is demonstrated in Figure (3). Elastic limit pressure obtained by HSDT has magnificent adaption with the FEM ones. However, elastic limit pressure obtained by FSDT has a significant difference with FEM results. The FSDT cannot predict the onset of the yield accurately.

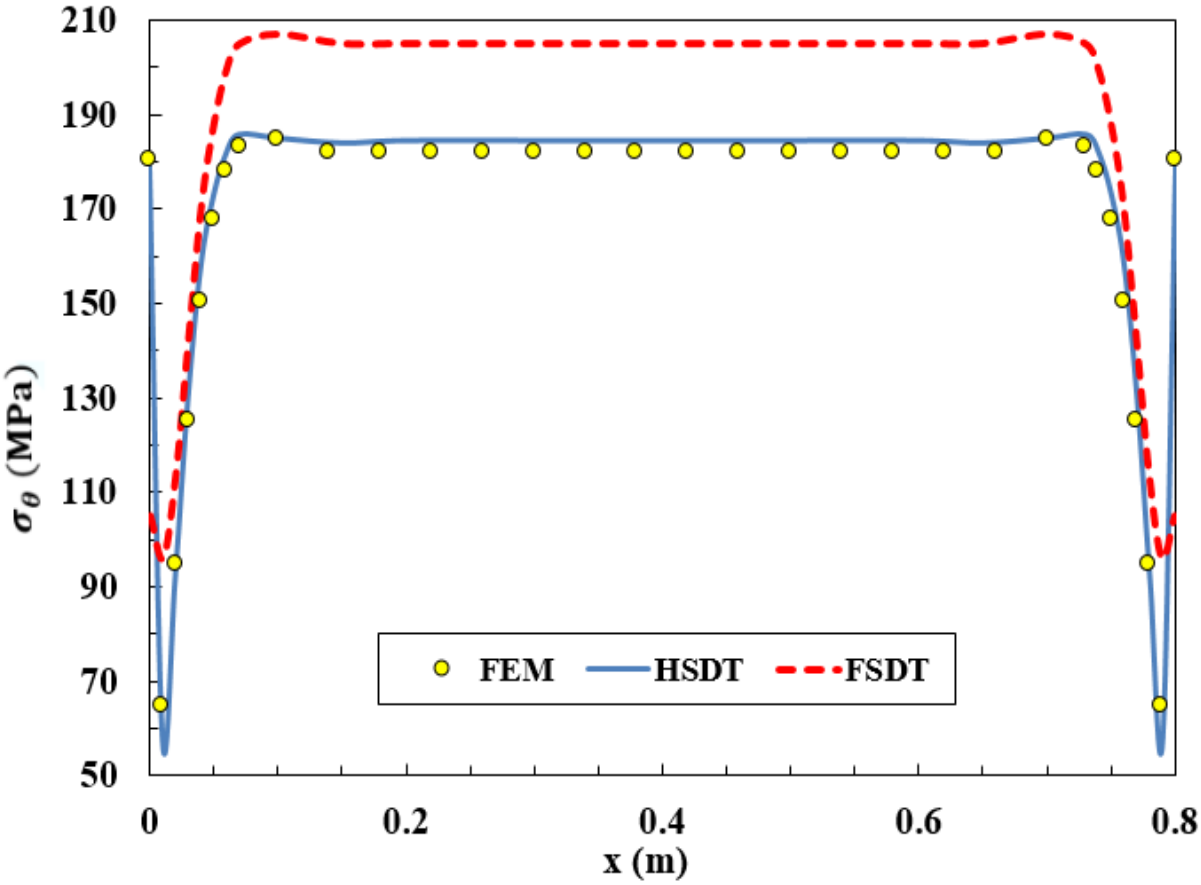
210
190
170
150
130
110
90
70
50
σ_θ (MPa)
0
0.2
0.4
0.6
0.8
x (m)
FEM
HSDT
FSDT

(a)

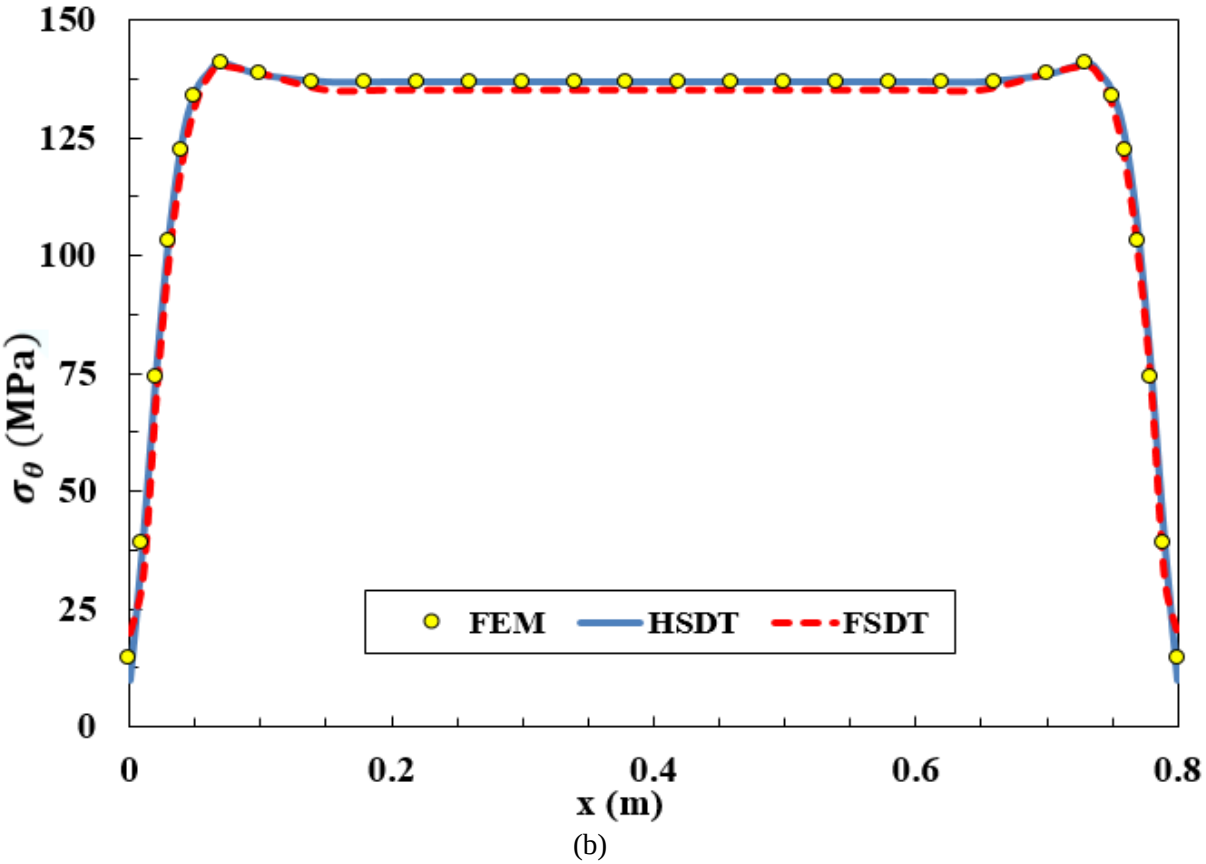
150
125
100
75
50
25
0
σ_θ (MPa)
0
0.2
0.4
0.6
0.8
x (m)
FEM
HSDT
FSDT

(b)

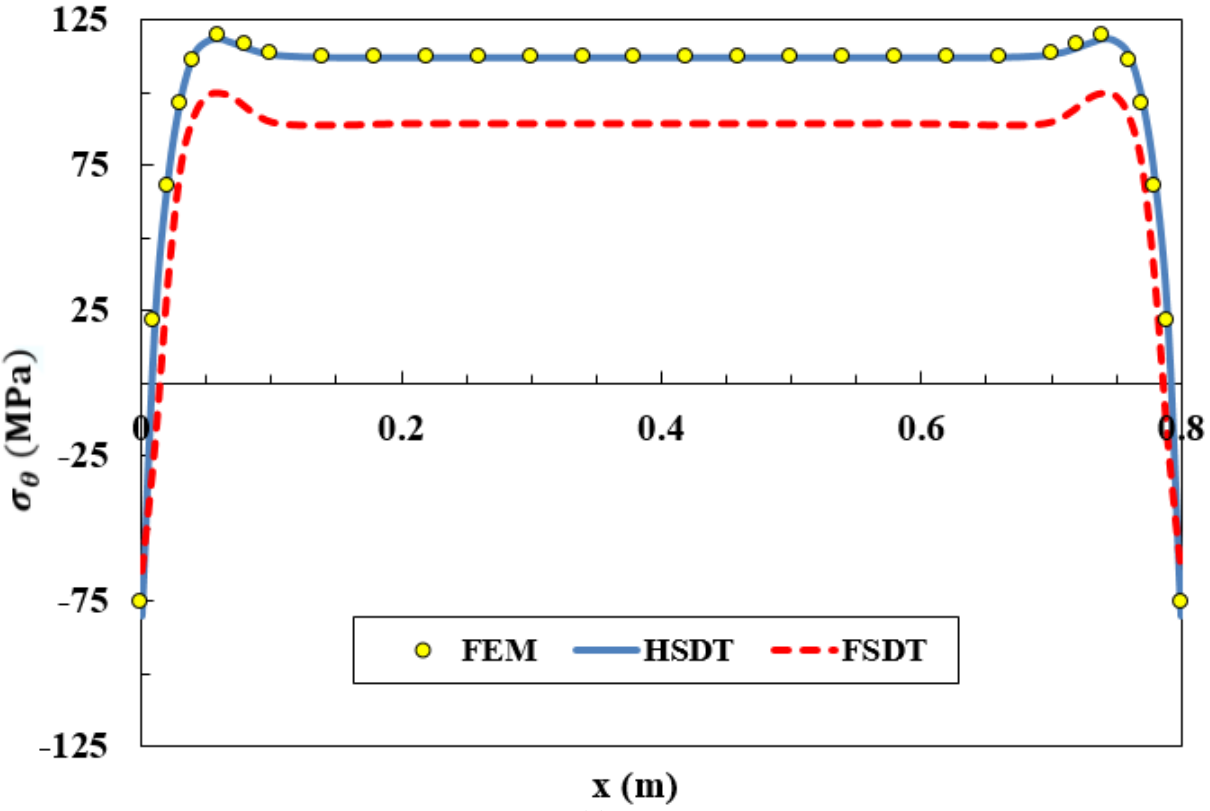

(c)

Figure 2 Circumferential stress distribution along the length of the shell subjected to $P = 70\ MPa$ at (**a**) inner surface (**b**) middle surface (**c**) outer surface.

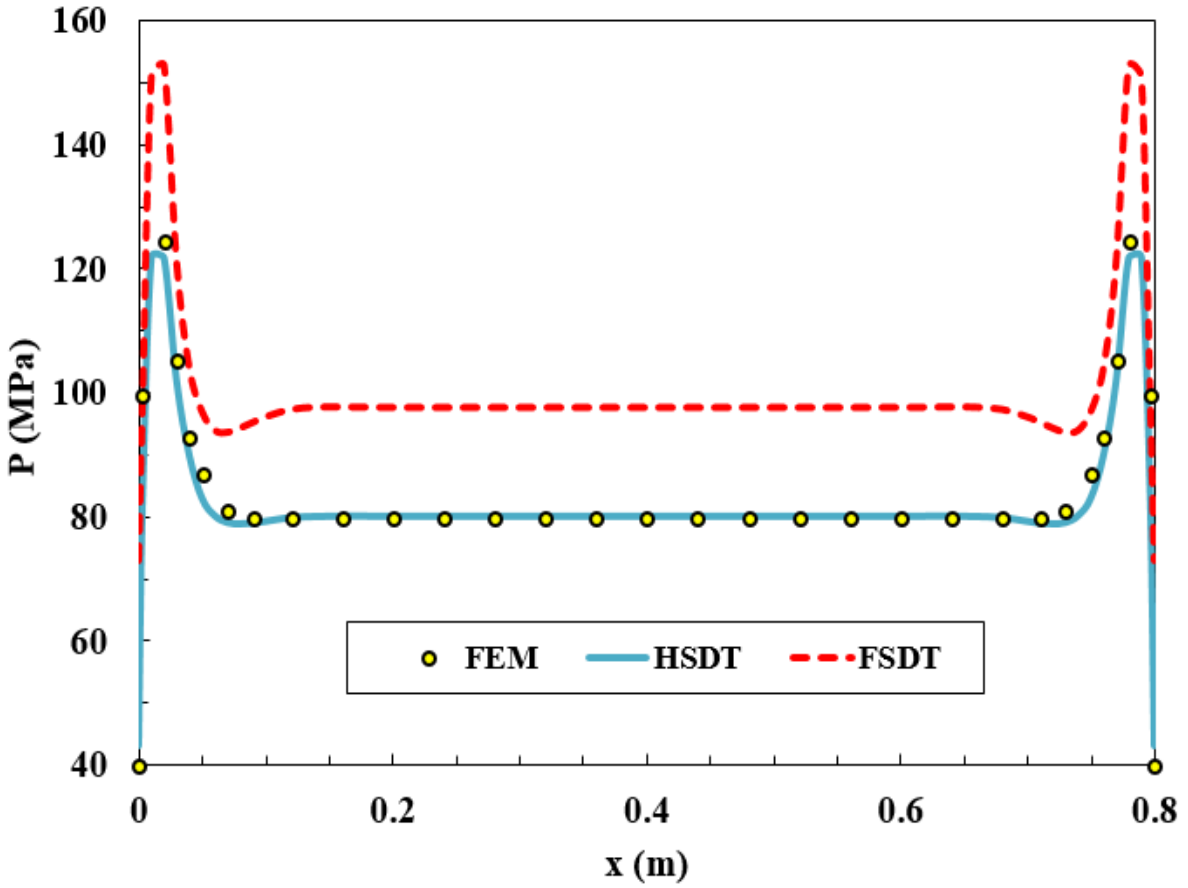

Figure 3 Elastic limit pressure along the length of the cylinder.

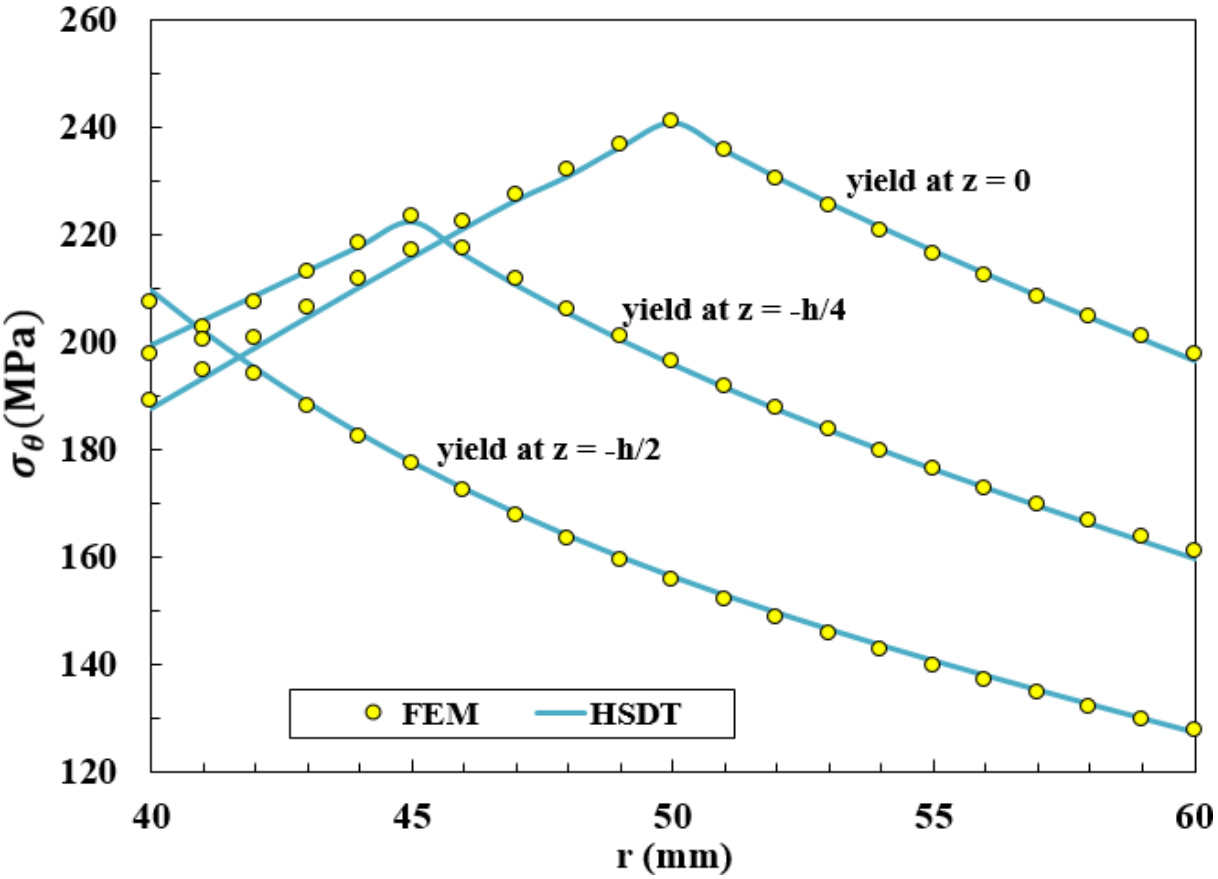

Figure 4 Elasto-plastic circumferential stress distribution along the thickness of the cylinder.

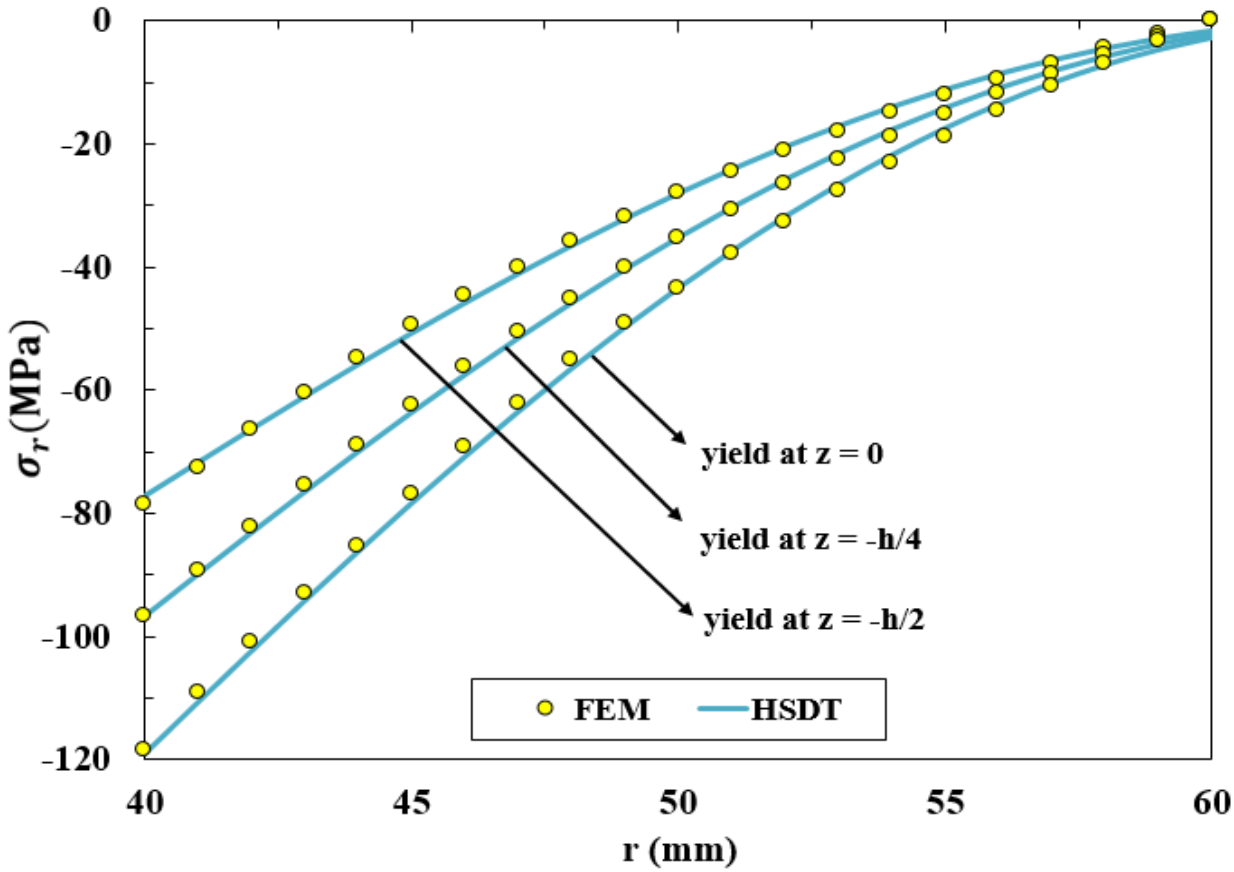

Figure 5 Elasto-plastic radial stress distributions along the thickness of the cylinder.

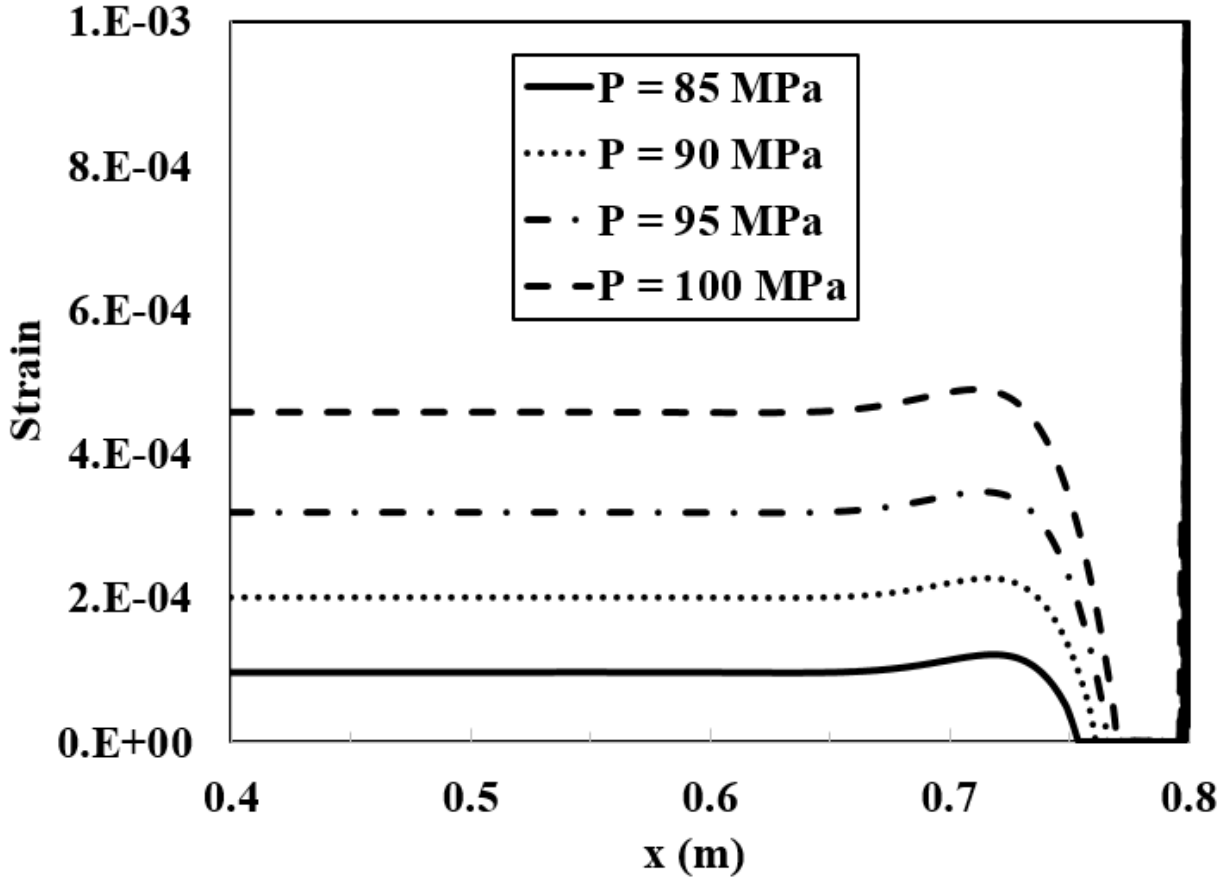

Figure 6 Strain distributions along the half length of the cylinder.

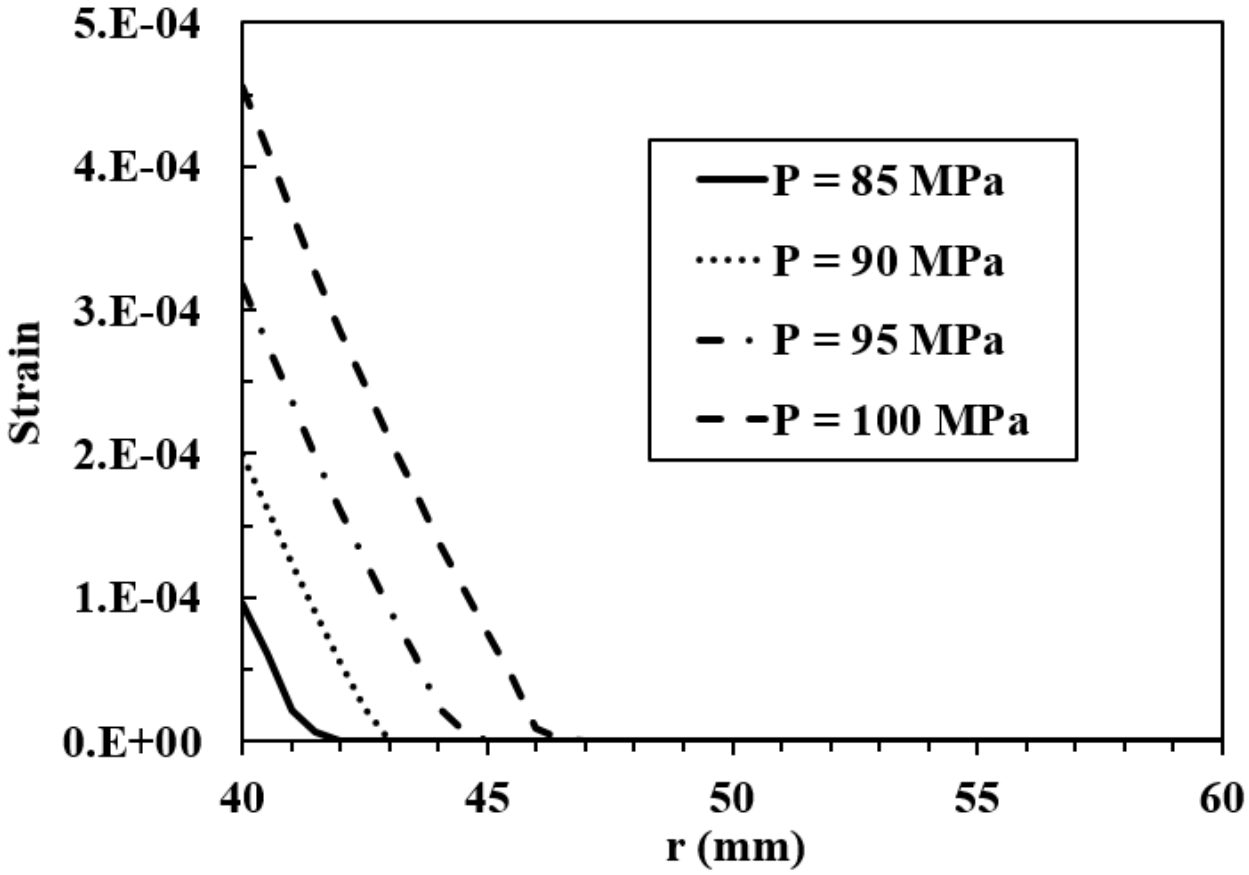

Figure 7 Strain distributions along the thickness of the cylinder.

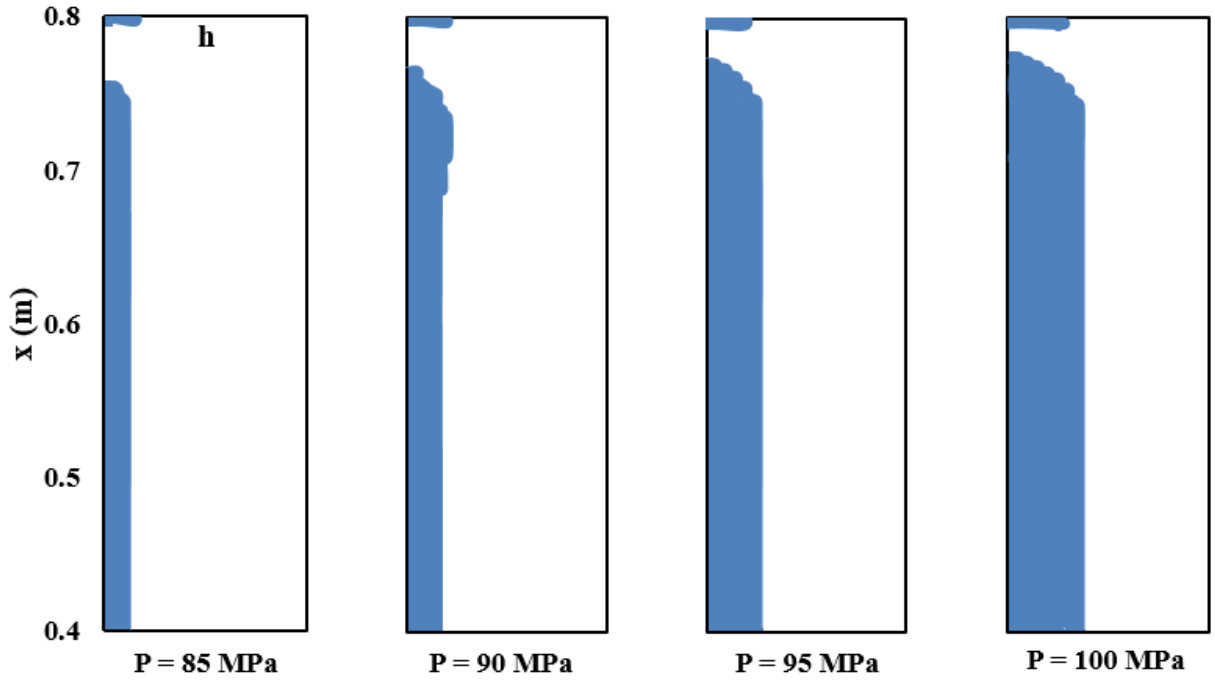

Figure 8 Plastic zone of the cylinder under different pressure.

Figures (4) and (5) are illustrated the circumferential and radial stress distribution at the middle length along the thickness of the cylindrical shell using HSDT. As shown in these Figures the stress distributions of the cylinder are plotted for three states that the cylinder is yielded at the inner surface ($z = -h/2$), $z = -h/4$, and middle surface ($z = 0$). The peaks shown in Figure (4) indicate the yield point of the cylinder in the radial direction. Before this point the cylinder is plastic and after this point the cylinder behave elastic. The results reveal that the elasto-plastic stress analysis obtained using HSDT has acceptable precision, especially near the inner surface where yielding begins.

The strain distribution along the inner surface and half length of the cylinder due to its symmetry condition are shown in Figure (6) for different values of inner pressure. As shown in this Figure by increasing the inner pressure the plastic strain zone of the cylinder enhanced. Figure (7) shows the strain amounts along the thickness of the cylinder at the middle length of it for different values of the inner pressure. It is clear that by increasing of the inner pressure the depth of lead to growth of the plastic zone. At a pressure of 85 MPa, almost 10% of the cylinder thickness has changed to plastic, while at a pressure of 100 MPa, about 35% of the thickness of the cylinder has become plastic. Figure (8) is shown the plastic zone of the half length of cylinder under the pressure 85 to 100 MPa with the step of 5 MPa.

5 Conclusion

In this paper elasto-plastic stress analysis and elastic limit pressure of clamped-clamped axisymmetric cylindrical shells subjected to internal pressure are studied. The case study for the cylinder shell was done based on von Mises yield criterion and the shell was assumed made of elastic-perfectly plastic material. The Prandtl-Reuss flow rule and the radial return method are used to derive the stress after the cylinder starts the plastic deformation. The following conclusions are achieved from the present study.

Plane elasticity theory (PET) can only cover the stress and displacement along the thickness, away from the edges of the cylinder, because this theory cannot consider the shear deformation. Therefore, this theory is not appropriate for elasto-plastic analyzing the cylinder through the length.

The boundary conditions used to obtain the constants for PET are in the terms of stresses at the inner and outer surfaces of the cylinder. Hence, circumferential stress obtained using PET is more accurate than HSDT ones through the thickness, at the middle length of the cylinder. On the contrary, the boundary conditions used to obtain the constants for HSDT are in the terms of displacements. Accordingly, radial displacement achieved by HSDT is more precise than PET ones.

The FSDT is not accurate enough for the stress analysis of the cylinder. The shear stress is uniform across the thickness of the shell for FSDT. This cannot be precise since the shear stress is known to be parabolic. Only the higher-order shear deformation theories are capable of reproducing the parabolic behavior of the transverse shear stress and satisfying the tangential traction-free conditions on the inner and outer surfaces of the shell. If the shell becomes thinner the stresses and displacements of the shell obtained based on FSDT and HSDT are converges.

The elastic limit pressure obtained by PET can be used away from the boundary of the clamped-clamped cylindrical shell. Shear deformation theories are needed for elasto-plastic analysis through the length of the shell. The elastic limit pressure along the length of the shell predicted by HSDT is more accurate than that of FSDT. In addition, since the FSDT cannot predict the elastic limit pressure correctly, it cannot be proper for elasto-plastic stress analysis of the thick-walled shell. The elasto-plastic stress analysis obtained from HSDT has acceptable precision with FEM results.

References

[1] P. L. Gould, and Y. Feng, "*Introduction to Linear Elasticity"*, Vol. 2, Springer, New York: Springer-Verlag, USA, 1994, https://doi.org/10.1007/978-3-319-73885-7.

[2] C. R. Calladine, "*Theory of Shell Structures"*, Cambridge University Press, New York, USA,1983.

[3] M. Ghannad, and M. Z. Nejad, "Complete Eastic Solution of Pressurized Thick Cylindrical Shells Made of Heterogeneous Functionally Graded Materials," *Mechanics*, Vol. 18, No. 6, pp. 640-649, 2012, doi: https://doi.org/10.5755/j01.mech.18.6.3158.

[4] I. Mirsky, and G. Herrmann, "Axially Symmetric Motions of Thick Cylindrical Shells," 1958, Vol. 25, No. 1, pp. 97-102, *Journal of Applied Mechanics*, doi: https://doi.org/10.1115/1.4011695.

[5] J. Reddy, and C. Liu, "A Higher-order Shear Deformation Theory of Laminated Elastic Shells," *International Journal of Engineering Science*, Vol. 23, No. 3, pp. 319-330, 1985, doi: https://doi.org/10.1016/0020-7225(85)90051-5.

[6] M. Ghannad, and M. Z. Nejad, "Elastic Analysis of Heterogeneous Thick Cylinders Subjected to Internal or External Pressure using Shear Deformation Theory," *Acta Polytechnica Hungarica*, Vol. 9, No. 6, pp. 117-136, 2012, DOI: 10.12700/APH.9.6.2012.6.8.

[7] H. Eipakchi, G. Rahimi, and S. E. Khadem, "Closed form Solution for Displacements of Thick Cylinders with Varying Thickness Subjected to Non-uniform Internal Pressure," *Structural Engineering and Mechanics*, Vol. 16, No. 6, pp. 731-748, 2003, doi: https://doi.org/10.12989/sem.2003.16.6.731.

[9] H. Gharooni, and M. Ghannad, "Nonlinear Analytical Solution of Nearly Incompressible Hyperelastic Cylinder with Variable Thickness under Non-uniform Pressure by Perturbation Technique," *Journal of Computational Applied Mechanics,* Vol. 50, No. 2, pp. 395-412, 2019, doi: https://doi.org/10.22059/JCAMECH.2019.276286.364.

[10] H. Gharooni, and M. Ghannad, "Nonlinear Analysis of Radially Functionally Graded Hyperelastic Cylindrical Shells with Axially-varying Thickness and Non-uniform Pressure Loads Based on Perturbation Theory," *Journal of Computational Applied Mechanics,* Vol. 50, No. 2, pp. 324-340, 2019, doi: https://doi.org/10.22059/JCAMECH.2019.282149.401.

[11] A. Nadai, "*Theory of Fracture and Flow of Solids"*, United Engineering Trustees Inc., Book Co., New York, McGraw-Hill, 1950, https://doi.org/10.1115/1.3636654.

[12] J. Chakrabarty, "*Theory of Plasticity"*, Third Edition, Butterworth-Heinemann, UK: Elsevier, 2006.

[13] A. N. Eraslan, "On the Linearly Hardening Rotating Solid Shaft," *European Journal of Mechanics-A/Solids,* Vol. 22, No. 2, pp. 295-307, 2003, doi: https://doi.org/10.1016/S0997-7538(02)00002-5.

[14] A. N. Eraslan, "Elastoplastic Deformations of Rotating Parabolic Solid Disks using Tresca's Yield Criterion," *European Journal of Mechanics-A/Solids,* Vol. 22, No. 6, pp. 861-874, 2003, doi: https://doi.org/10.1016/S0997-7538(03)00068-8.

[15] A. Prokudin, "Exact Elastoplastic Analysis of a Rotating Cylinder with a Rigid Inclusion under Mechanical Loading and Unloading," *ZAMM- Journal of Applied Mathematics and Mechanics/Zeitschrift für Angewandte Mathematik und Mechanik,* Vol. 100, No. 3, p. e201900213, 2020, doi: https://doi.org/10.1002/zamm.201900213.

[16] M. Z. Nejad, A. Rastgoo, and A. Hadi, "Exact Elasto-plastic Analysis of Rotating Disks Made of Functionally Graded Materials," *International Journal of Engineering Science,* Vol. 85, pp. 47-57, 2014, doi: https://doi.org/10.1016/j.ijengsci.2014.07.009.

[17] Q. Zhu, S. Wang, D. F. Zhang, Y. J. Jiang, and X. Yue, "Elastoplastic Analysis of Ultimate Bearing Capacity for Multilayered Thick-walled Cylinders under Internal Pressure," *Strength of Materials,* Vol. 52, pp. 521-531, 2020, doi: https://doi.org/10.1007/s11223-020-00203-9.

[18] A. Temesgen, S. Singh, and T. Pankaj, "Elastoplastic Analysis in Functionally Graded Thick-walled Rotating Transversely Isotropic Cylinder under a Radial Temperature Gradient and Uniform Pressure," *Mathematics and Mechanics of Solids,* Vol. 26, No. 1, pp. 5-17, 2021, doi: https://doi.org/10.1177/1081286520934041.

[19] G. Scalet, and F. Auricchio, "Computational Methods for Elastoplasticity: An Overview of Conventional and Less-conventional Approaches," *Archives of Computational Methods in Engineering*, Vol. 25, pp. 545-589, 2018, doi: https://doi.org/10.1007/s11831-016-9208-x.

[20] M. L. Wilkins, *"Calculation of Elastic-plastic Flow"*, University of California, Ernest L. Lawrence Radiation Laboratory, Vol. 7322, 1969.

[21] B. Loret, and J. H. Prevost, "Accurate Numerical Solutions for Drucker-Prager Elastic-plastic Models," *Computer Methods in Applied Mechanics and Engineering*, Vol. 54, No. 3, pp. 259-277, 1986, doi: https://doi.org/10.1016/0045-7825(86)90106-4.

[22] P. J. Yoder, and R. G. Whirley, "On the Numerical Implementation of Elastoplastic Models," *Journal of Applied Mechanics*, Vol. 51, No. 2, pp. 283-288, 1984, doi: https://doi.org/10.1115/1.3167613.

[23] F. Dunne, "*Introduction to Computational Plasticity"*, New York: Oxford University Press, 2006.

[24] G. Widłak, "Radial Return Method Applied in Thick-walled Cylinder Analysis," *Journal of Theoretical and Applied Mechanics*, Vol. 48, No. 2, pp. 381-395, 2010, http://warminski.pollub.plwww.ptmts.org.pl/jtam/index.php/jtam/article/view/v48n2p381.

[25] A. Mendelson, *"Plasticity; Theory and Application"*, Macmillan Series in Applied Mechanics, New York: Macmillan, ISBN: 0898745829, 1968, Radial return method applied in thick-walled cylinder analysis | Widłak | Journal of Theoretical and Applied Mechanics.

[26] H. Gharooni, M. Ghannad, and M. Z. Nejad, "Thermo-elastic Analysis of Clamped-Clamped Thick FGM Cylinders by using Third-order Shear Deformation Theory," *Latin American Journal of Solids and Structures*, Vol. 13, pp. 750-774, 2016, doi: https://doi.org/10.1590/1679-78252254.

Appendix A

$$[A]=\begin{bmatrix}0 & 0 & 0 & 0\\ 0 & (1-\nu)\dfrac{Rh^3}{12} & 0 & 0\\ 0 & 0 & \mu Rh & \mu\dfrac{h^3}{12}\\ 0 & 0 & \mu\dfrac{h^3}{12} & \mu\dfrac{Rh^3}{12}\end{bmatrix} \tag{A1}$$

$$[B]=\begin{bmatrix}0 & (1-\nu)\dfrac{h^3}{12} & 0 & 0\\ (1-\nu)\dfrac{h^3}{12} & 0 & -\mu Rh & -(\mu-2\nu)\dfrac{h^3}{12}\\ 0 & \mu Rh & 0 & 0\\ 0 & (\mu-2\nu)\dfrac{h^3}{12} & 0 & 0\end{bmatrix} \tag{A2}$$

$$[C]=\begin{bmatrix}(1-\nu)Rh & 0 & \nu h & \nu Rh\\ 0 & -\mu Rh & 0 & 0\\ -\nu h & 0 & -(1-\nu)\alpha & (1-\nu)R\alpha-h\\ -\nu Rh & 0 & (1-\nu)R\alpha-h & -(1-\nu)R^2\alpha\end{bmatrix} \tag{A3}$$

$$\{F\}=\frac{1}{(1+\nu)(1-2\nu)E}\begin{bmatrix}C_0 & 0 & -P\left(R-\dfrac{h}{2}\right) & P\dfrac{h}{2}\left(R-\dfrac{h}{2}\right)\end{bmatrix}^T \tag{A4}$$

Where

$$\mu=\frac{K}{2}(1-2\nu)$$

$$\alpha=\ln\left(\frac{R+h/2}{R-h/2}\right)$$

Appendix B

$$[A]=\begin{bmatrix}[A_1]_{4\times4} & [A_2]_{4\times4}\\ [A_3]_{4\times4} & [A_4]_{4\times4}\end{bmatrix} \tag{B1}$$

$$[B]=\begin{bmatrix}[B_1]_{4\times4} & [B_2]_{4\times4}\\ [B_3]_{4\times4} & [B_4]_{4\times4}\end{bmatrix} \tag{B2}$$

$$[C]=\begin{bmatrix}[C_1]_{4\times4} & [C_2]_{4\times4}\\ [C_3]_{4\times4} & [C_4]_{4\times4}\end{bmatrix} \tag{B3}$$

$$[A_2]=[A_3]=[B_4]=[0]_{4\times4} \tag{B4}$$

$$[A_1] = (1-\nu)\begin{bmatrix} 0 & 0 & 0 & 0 \\ 0 & \frac{Rh^3}{12} & \frac{h^5}{80} & \frac{Rh^5}{80} \\ 0 & \frac{h^5}{80} & \frac{Rh^5}{80} & \frac{h^7}{448} \\ 0 & \frac{Rh^5}{80} & \frac{h^7}{448} & \frac{Rh^7}{448} \end{bmatrix} \tag{B5}$$

$$[A_4] = \frac{(1-2\nu)}{2}\begin{bmatrix} Rh & \frac{h^3}{12} & \frac{Rh^3}{12} & \frac{h^5}{80} \\ \frac{h^3}{12} & \frac{Rh^3}{12} & \frac{h^5}{80} & \frac{Rh^5}{80} \\ \frac{Rh^3}{12} & \frac{h^5}{80} & \frac{Rh^5}{80} & \frac{h^7}{448} \\ \frac{h^5}{80} & \frac{Rh^5}{80} & \frac{h^7}{448} & \frac{Rh^7}{448} \end{bmatrix} \tag{B6}$$

$$[B_1] = (1-\nu)\begin{bmatrix} 0 & \frac{h^3}{12} & \frac{Rh^3}{12} & \frac{h^5}{80} \\ \frac{h^3}{12} & 0 & 0 & 0 \\ \frac{Rh^3}{12} & 0 & 0 & 0 \\ \frac{h^5}{80} & 0 & 0 & 0 \end{bmatrix} \tag{B7}$$

$$[B_2] = -[B_3]^T = \begin{bmatrix} 0 & 0 & 0 & 0 \\ \nu Rh - \frac{Rh}{2} & \frac{\nu h^3}{4} - \frac{h^3}{24} & \frac{\nu Rh^3}{4} - \frac{Rh^3}{24} & \frac{\nu h^5}{16} - \frac{h^5}{160} \\ \frac{\nu h^3}{4} - \frac{h^3}{12} & \frac{\nu Rh^3}{4} - \frac{Rh^3}{12} & \frac{\nu h^5}{16} - \frac{h^5}{80} & \frac{\nu Rh^5}{16} - \frac{Rh^5}{80} \\ \frac{\nu Rh^3}{4} - \frac{Rh^3}{8} & \frac{\nu h^5}{16} - \frac{3h^5}{160} & \frac{\nu Rh^5}{16} - \frac{3Rh^5}{160} & \frac{\nu h^7}{64} - \frac{3h^7}{896} \end{bmatrix} \tag{B8}$$

$$[C_1] = \begin{bmatrix} Rh(\nu-1) & 0 & 0 & 0 \\ 0 & \frac{Rh}{2}(2\nu-1) & \frac{h^3}{12}(2\nu-1) & \frac{Rh^3}{8}(2\nu-1) \\ 0 & \frac{h^3}{12}(2\nu-1) & \frac{Rh^3}{6}(2\nu-1) & \frac{3h^5}{80}(2\nu-1) \\ 0 & \frac{Rh^3}{8}(2\nu-1) & \frac{3h^5}{80}(2\nu-1) & \frac{9Rh^5}{160}(2\nu-1) \end{bmatrix} \tag{B9}$$

$$[C_2] = -[C_3]^T = \begin{bmatrix} \nu h & \nu R h & \frac{\nu h^3}{4} & \frac{\nu R h^3}{4} \\ 0 & 0 & 0 & 0 \\ 0 & 0 & 0 & 0 \\ 0 & 0 & 0 & 0 \end{bmatrix} \tag{B10}$$

$$[C_4] = \begin{bmatrix} -(1-\nu)\alpha & (1-\nu)R\alpha - h \\ (1-\nu)R\alpha - h & -R^2(1-\nu)\alpha \\ -R(1-\nu)(R\alpha - h) & R^2(1-\nu)(R\alpha - h) - \frac{h^3}{4} \\ R^2(1-\nu)(R\alpha - h) - \frac{h^3}{12}(1-2\nu) & -R^3(1-\nu)\left(R\alpha - h + \frac{h^3}{6R^2}\right) \\ -R(1-\nu)(R\alpha - h) & R^2(1-\nu)(R\alpha - h) - \frac{h^3}{12}(1-2 \\ R^2(1-\nu)(R\alpha - h) - \frac{h^3}{4} & -R^3(1-\nu)\left(R\alpha - h + \frac{h^3}{6R^2}\right) \\ -R^3(1-\nu)\left(R\alpha - h + \frac{h^3}{4R^2}\right) & R^4(1-\nu)\left(R\alpha - h - \frac{h^3}{12R^2}\right) - \frac{h^5}{80}(7 \\ R^4(1-\nu)\left(R\alpha - h - \frac{h^3}{12R^2}\right) - \frac{h^5}{80}(7-2\nu) & -R^5(1-\nu)\left(R\alpha - h + \frac{h^3}{12R^2} + \frac{h}{10}\right. \end{bmatrix}$$

Where

$$\alpha = \ln\left(\frac{2R+h}{2R-h}\right)$$

$$\{F\} = \frac{1}{(1+\nu)(1-2\nu)E}\begin{bmatrix} C_0 & 0 & 0 & 0 & -P\left(R - \frac{h}{2}\right) & P\frac{h}{2}\left(R - \frac{h}{2}\right) & -P\frac{h^2}{4}\left(R - \frac{h}{2}\right) \end{bmatrix} \tag{B12}$$